

Optimization and simulation of low-temperature combustion and heat transfer in an Uhde carbonization furnace

Jun Liu¹ · Yongfa Zhang¹ · Ying Wang¹ · Lei Chen¹ · Gaihuan Liu¹

Received: 26 March 2015 / Accepted: 24 November 2015 / Published online: 8 December 2015
© Springer-Verlag Berlin Heidelberg 2015

Abstract The temperature distribution inside a low-temperature combustion chamber with circuited flame path during the low temperature pyrolysis of lignite was simulated using the computational fluid dynamics software FLUENT. The temperature distribution in the Uhde combustion chamber showed that the temperature is very non-uniform and could therefore not meet the requirements for industrial heat transfer. After optimizing the furnace, by adding a self-made gas-guide structure to the heat transfer section as well as adjusting the gas flow size in the flame path, the temperature distribution became uniform, and the average temperature (550–650 °C) became suitable for industrial low-temperature pyrolysis. The Realizable k-epsilon model, P-1 model, and the Non-premixed model were used to calculate the temperature distribution for the combustion of coke-oven gas and air inside the combustion chamber. Our simulation is consistent with our experimental results within an error range of 40–80 °C. The one-dimensional unsteady state heat conduction differential equation $\rho_{coal} C_{coal} \frac{\partial T}{\partial t} = \frac{\partial}{\partial x} (\lambda \frac{\partial T}{\partial x})$ can be used to calculate the heat transfer process. Our results can serve as a first theoretical base and may enable technological advances with regard to lignite pyrolysis.

Electronic supplementary material The online version of this article (doi:10.1007/s00231-015-1727-8) contains supplementary material, which is available to authorized users.

✉ Yongfa Zhang
yongfaz@tyut.edu.cn

¹ Key Laboratory of Coal Science and Technology, Ministry of Education and Shanxi Province, Taiyuan University of Technology, Taiyuan 030024, China

List of symbols

a	The three-dimensional length of the exhaust gas outlet (mm)
b	The three-dimensional width of the exhaust gas outlet (mm)
C	The linear anisotropic phase function coefficient
C	The specific heat (J K/kg)
$C_{1\epsilon}$	The default value determined from experiments for fundamental turbulent flows
C_2	The default value determined from experiments for fundamental turbulent flows
D_1	The three-dimensional outside diameter of the fuel inlet (mm)
D_2	The three-dimensional outside diameter of the air inlet (mm)
G	The three-dimensional incident radiation
G_k	The turbulent energy which was resulted from mean velocity gradient
G_b	The turbulent energy affected by buoyancy
h	The enthalpy (J/kg)
I	The radiation intensity
k	The kinetic energy
L	The three-dimensional diameter of the combustion chamber
q_r	The three-dimensional radiation heat flux
S_K	The user-defined source terms
S_ϵ	The user-defined source terms
S_ϕ	A generalized source term
T	The carbonization temperature (°C)
T_{fuel}	The inlet temperature of the fuel (K)
T_{air}	The inlet temperature of the fuel (K)
T_{ref}	A user input for PDF models (K)
t	The carbonization time (sec or min)
\vec{u}	The three-dimensional mean velocity of fluid-flow (m/s)

V	The three-dimensional volumetric flow rate of fuel or air (m^3/h)
x	The two-dimensional heat transfer distance (mm or m)
Y_M	The compressible turbulent fluctuating inflation's effect on the total dissipation rate

Greek symbols

ϕ	A variable
Γ	A generalized diffusion coefficient corresponding to variable ϕ
α	The absorption coefficient
σ_s	The scattering coefficient
σ_k	The turbulent Prandtl numbers for k
σ_ε	The turbulent Prandtl numbers for ε
ω_i	The mass fraction of the element i
ω_{io}	The value of oxidizer inlet
ω_{if}	The value of fuel flow at the entrance
σ_ε	The default value determined from experiments for fundamental turbulent flows
ω	The mixture fraction
ρ	The density of solid coal/coke or gas ($\text{kg}\cdot\text{m}^{-3}$)
ε	The dissipation rate
λ	Heat conductivity coefficient ($\text{W}/\text{m}\cdot\text{K}$)
κ_{eff}	The effective thermal conductivity ($\text{W}/(\text{m}\cdot\text{K})$)

Subscripts

ad	Air dried base
daf	Dry ash free base
eff	Effective
i	1,2,3...
io	The oxidizer inlet
if	The fuel inlet
t	Total

1 Introduction

Large reserves, more than 56.1 billion tons of low-rank coal resources like lignite, long flame coal and non-caking coal are proved to exist in China. Among these resources, the proved reserves of lignite are more than 13 billion tons [1]. Therefore, the technology which converts low-rank coal efficiently to alternative fuel is commercially important. The low-temperature pyrolysis of coal is an important technology for utilizing low-rank coal. During the process, coal is transformed into pyrolysis gas, low-temperature tar and semi-coke by heating up to 500–600 °C while ensuring air isolation or non-oxidation [2–6]. Extensive research and development of low temperature pyrolysis for low-rank coal is carried out by researchers all over the world [7–9].

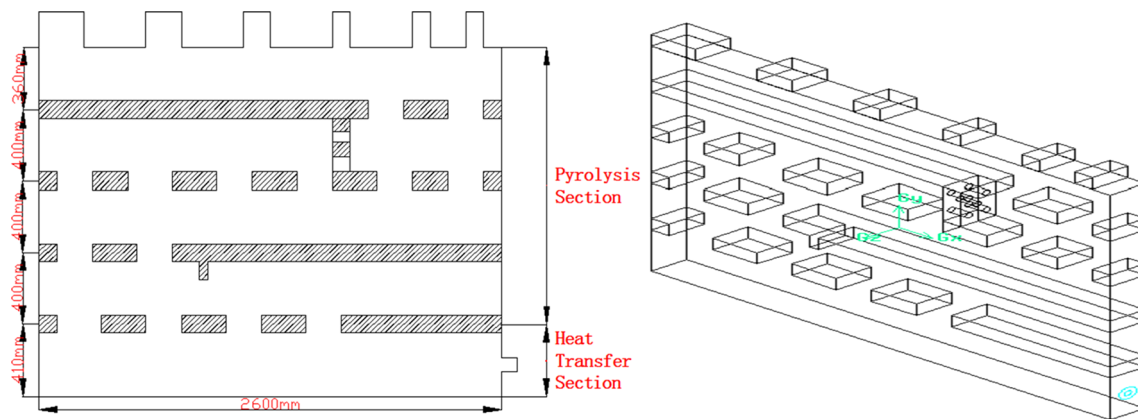
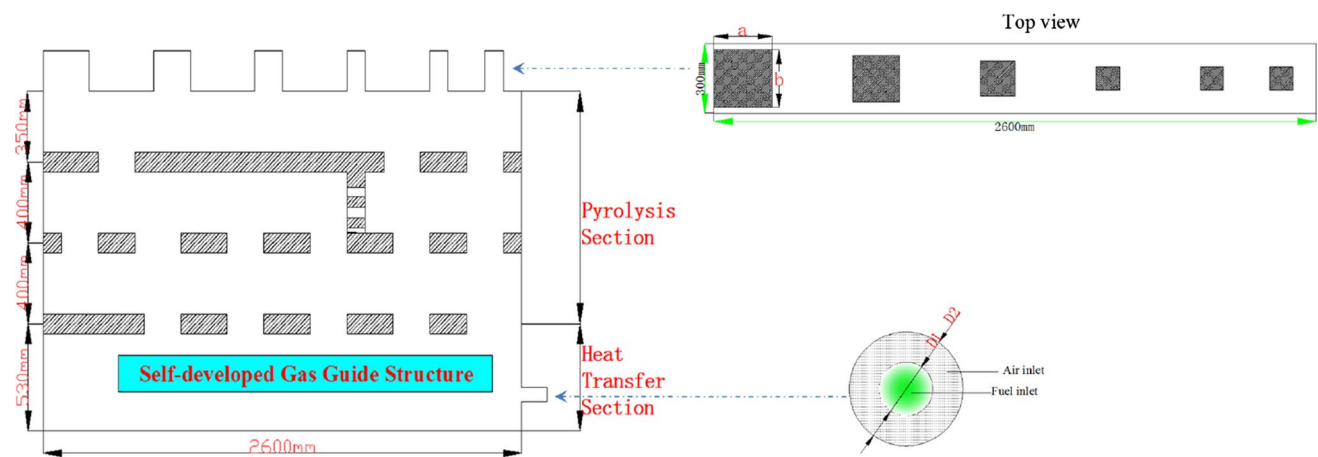
The Uhde furnace is a continuous externally heated vertical pyrolysis oven, which was designed by British Uhde Company in 19th century. It has been reformed for producing coal-oven gas and its coke byproduct after its introduction to China in the 80s. Two types of flame-structures can be used in the combustion chamber. One is the vertical flame path with its upward or downward orientation in which the gas flow resistance is small. The other is the circuited flame path with a segmented heating structure in which the gas flows like a “snake”. The latter transfers heat slowly which can reduce the temperature difference between the upper and lower layers in the carbonization furnace [10].

The disadvantages of the Uhde furnace with the circuited flame are: (1) The temperature difference along the flame path in each layer is too high to meet the requirements for low temperature pyrolysis in the range of 500–600 °C. (2) Because of the high temperature needed for the production of coke, the overall gas consumption is large. Reducing the gas consumption for the low temperature combustion chamber leads to a non-uniform distribution of temperature. In order to reach the desired temperature range of 500–600 °C, a low-temperature combustion chamber with a circuited flame path was developed by our team. In addition, a heat resisting silica brick was used to produce this section. By adding our gas guide-structure (at the base of the furnace) and adjusting the gas flow size in the flame path, the circuited flame path could be optimized. This enables a more uniform temperature distribution throughout the pyrolysis area, and hence satisfies the industrial requirements. In the upper part of the circulated combustion chamber, a vertical flue was selected, and high thermal conductivity cast iron was used to manufacture the thin chamber wall.

Łukasz et al. [11] developed a validated coupled CFD model of a coke oven battery and analyzed the thermal processes within coke oven charge. A two dimensional transient model of coal carbonization was developed by Wei et al. [12] to simulate the coking process including heat transfer and fluid flow in the coking chamber. Raiee et al. [13] had studied the optimization of the angle of curvature for a Ranque–Hilsch vortex tube, using both experimental and Reynolds stress turbulence numerical modeling. The numerical study was done by full 3D steady-state CFD-simulation with FLUENT 6.3.26. However, until now, only a few studies describe the flow and heat transfer processes in the low temperature carbonization furnace by means of numerical simulation [14–16]. In this work, we used a commercial software package (ANSYS Fluent) to calculate not only the internal temperature field distribution in the optimized Uhde furnace but also the heat transfer process in the low temperature carbonization furnace.

Table 1 The main concentration of COG (V %)

Component	CH ₄	CO	C ₂ H ₄	C ₂ H ₆	CO ₂	N ₂	O ₂	H ₂
Volume%	25.5	6.0	1.7	0.5	2.4	4.0	0.4	59.5

**Fig. 1** The structure of the combustion chamber in the Uhde furnace**Fig. 2** The structure of the optimized combustion chamber

2 Experimental

2.1 Fuel gas composition

The composition of the fuel gas, coke oven gas (COG) is shown in Table 1.

2.2 Combustion chamber

The combustion chamber is cuboid and the exhaust gas outlet is at the top. The double-pipe burner is located on the side of the chamber. The non-optimized combustion chamber (2600 × 300 × 1960 mm) is shown in Fig. 1. The structure of the low-temperature combustion chamber (2600 × 300 × 1680 mm) after simulation

optimization and experimental verification is shown in Fig. 2.

3 Numerical model

3.1 Mesh size and boundary conditions

The geometric model of the combustion chamber is divided into a small grid using the regional method [17]. The method helps to divide complex physical domains or topological structures into a simple grid (the structure block of a grid) according to individual shapes. Both fuel and air-inlet of the combustion chamber were divided using the T-grid method to form a tetrahedral grid. The furnace (rectangle

Table 2 Interval size and mesh number

	Interval size/m	Mesh number
Uhde combustion chamber	0.02	29232
Optimized combustion chamber	0.02	26651
Carbonization furnace	0.02	28320

part) was divided using the Hex/Wedge copper method [18] to form a hexahedral grid. The different interval sizes and mesh numbers are shown in Table 2.

The circle channel (internal pipe) in the center of the nozzle was used for the delivery of coke -oven gas while the ring channel (external pipe) was used to supply air. Typically, the air excess coefficient of the coke oven was set in the range of 1.1–1.25 [19].

The same geometry size and fuel flow rate of the circulated combustion chamber were selected according to the industrial Uhde carbonization furnace. The flow rate of the COG was deduced from the production of semi-coke, which was calculated using the heat flux equilibrium. The flow rate of COG was chosen to be 32 m³/h. As shown in Fig. S1, the average temperature of the cuboid combustion chamber could achieve the maximum value by keeping the COG flow rate at 32 m³/h, which had been discovered in our previous study. The corresponding air coefficient is 1.25; the fuel and air-flow are 32 m³/h and 175 m³/h respectively. So 32 m³/h and 175 m³/h were selected as the flow rates of COG and air respectively, and the fuel diameter was 32 mm. The boundary conditions of the gas inlet, air inlet and gas outlet are all shown in Table 3 and correspond to Fig. 2.

3.2 Governing equations

General equation governing the conservation of mass, momentum, energy and species in gas phase and solid phase can be expressed as:

$$\frac{\partial}{\partial t}(\rho\phi) + \text{div}(\rho \vec{u} \phi) = \text{div}(\Gamma \text{grad}\phi) + S_\phi \tag{1}$$

where ρ is the (either solid coal/coke or gas) density in kg m⁻³, \vec{u} is the mean velocity in m s⁻¹, ϕ is a general variable, Γ is a generalized diffusion coefficient corresponding to variable ϕ , S_ϕ is a generalized source term.

Table 3 Parameters and the boundary conditions of the simulated operating conditions

Combustion chamber	Boundary conditions	Parameters
Fuel inlet	Velocity-inlet	$D_1 = 32 \text{ mm}, V_{\text{fuel}} = 32 \text{ m}^3/\text{h}, T_{\text{fuel}} = 293.15 \text{ K}$
Air inlet	Velocity-inlet	$D_1 = 32 \text{ mm}, D_2 = 80 \text{ mm}, V_{\text{air}} = 175 \text{ m}^3/\text{h}, T_{\text{air}} = 293.15 \text{ K}$
Exhaust gas outlet	Pressure-outlet	$a = b = 250, 200, 150, 100, 100, 100 \text{ mm}$

3.3 Model of combustion

3.3.1 Turbulence model

The turbulent modified model (Realizable k-ε model) [20] was selected as turbulent model. Turbulent kinetic energy and its dissipation rate transport equation for the Realizable k-ε model were presented as follows.

$$\frac{\partial}{\partial t}(\rho k) = \frac{\partial}{\partial x_i} \left[\left(\mu + \frac{\mu_t}{\sigma_k} \right) \frac{\partial k}{\partial x_i} \right] + G_k + G_b - \rho \varepsilon - Y_M + S_k \tag{2}$$

$$\begin{aligned} \frac{\partial}{\partial t}(\rho \varepsilon) = & \frac{\partial}{\partial x_i} \left[\left(\mu + \frac{\mu_t}{\sigma_\varepsilon} \right) \frac{\partial \varepsilon}{\partial x_i} \right] + \rho C_1 G S_\varepsilon \\ & - \rho C_2 \frac{\varepsilon^2}{k + \sqrt{\nu \varepsilon}} + C_{1\varepsilon} \frac{\varepsilon}{k} C_{3\varepsilon} G_b + S_\varepsilon \end{aligned} \tag{3}$$

where: $C_1 = \max \left[0.43, \frac{\eta}{\eta+5} \right]$, $\eta = S_\varepsilon^k$, $S = \sqrt{2S_{ij}S_{ij}}$ As shown in Eqs. (2) and (3), G_k represents the turbulent energy that results from the mean velocity gradient, G_b stands for the turbulent energy affected by buoyancy. Y_M is the compressible turbulent fluctuating inflation effect on the total dissipation rate. C_2 and $C_{1\varepsilon}$ are constant. σ_k and σ_ε are turbulent and the dissipation rate of turbulent Prandtl number respectively. In the software Fluent, $C_{1\varepsilon} = 1.44$, $C_2 = 1.9$, $\sigma_k = 1.0$, $\sigma_\varepsilon = 1.2$ are the default values (constant).

The Realizable k-ε turbulence model showed the best agreement with the experimental and analytical data available. The Realizable k-ε turbulence model is derived from the instantaneous Navier–Stokes equations [21]. The term “realizable” means that the model satisfies certain mathematical constraints on the Reynolds stresses and that it is consistent with the physics of turbulent flow. The analytical derivation of the Realizable k-ε turbulence model, its constants and additional terms and functions in the transport equations for k and ε are different from those in the standard k-ε and RNG k-ε models. This model can be used for different flow types, including spin-uniform shear flow, free flow (jet and mixing layer), cavity flow and boundary layer flow. For the simulation of round-shape jet and flat jet flow types, the Realizable k-ε model could give a better jet expansion angle. The turbulent modified model was chosen in our simulation.

3.3.2 Radiation model

Considering the non-premixed combustion of coke-oven gas and air reaching maximum temperature of 2300 K,

radiative heat transfer had to be taken into account. Our simulation used the P-1 radiation model. The P-1 radiation model is used to calculate the flux of the radiation inside the combustion chamber. It is the simplest case among the more general P-N radiation models derived from the expansion of the radiation intensity (I) into an orthogonal series of spherical harmonics [22–24]. If the former four sections of orthogonal spherical harmonic function are taken, the following equation can be obtained for the radiation heat flux q_r :

$$q_r = -\frac{1}{3(\alpha + \sigma_s) - C\sigma_s} \nabla G \quad (4)$$

here, α is the absorption coefficient, σ_s is the scattering coefficient, G is the incident radiation, C is the linear anisotropic phase function coefficient respectively.

Moreover, the P-1 model requires relatively little computing power and can be applied more readily to various complicated geometries. It is suitable for applications where the optical thickness (αL) is large (α is the absorption coefficient and L is the length scale of the domain). The absorption coefficient (α) can be a function of local concentrations of different species, path length and total pressure. On the other hand, the Weighted-Sum-of-Gray-Gases model (WSGGM) was chosen for calculating the variable absorption coefficient [25]. We used the default value of the convergence criteria for the P-1 model: 10^{-6} .

3.3.3 Model of non-premixed combustion

Coke-oven gas and air flow into the combustion chamber via separate paths. Hence, we used the Non-premixed combustion model in the simulation [26, 27]. The purpose of this model is not to solve every species transport equation, but to solve one or two conserved scalars (mixture fraction) of the transport equation, and then to derive the concentration of each component from the predicted mixture fraction. Under certain conditions, the transient thermal state of a fluid is important for a conserved quantity. The mixture fraction is characterized by ω , which originates from the element mass fraction of fuel flow.

$$\omega = \frac{\omega_i - \omega_{i,o}}{\omega_{i,f} - \omega_{i,o}} \quad (5)$$

Here ω_i stands for the mass fraction of the element i and $\omega_{i,o}$ stands for value of the oxidizer inlet while $\omega_{i,f}$ is the fuel flow at the entrance. The mixture fraction is a top mass fraction which is included in every component (CO_2 , H_2O , O_2 , etc.) including burned and unburned fuel flow elements. This approach is mainly used to simulate turbulent diffusion flames.

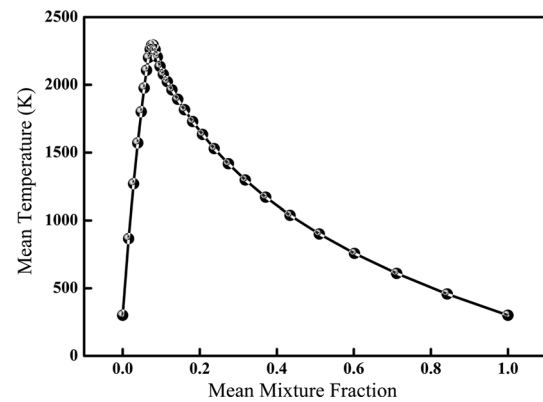


Fig. 3 Temperature dimensional change map and the mean mixture fraction

The non-premixed combustion model and Probability Density Function (PDF) were chosen for simulation of the chemical reaction. The non-premixed modeling approach offers many benefits over the finite rate formulation. This model allows intermediate (radical) species prediction, dissociation effects, and rigorous turbulence–chemistry coupling. The method is computationally efficient as it does not require the solution of a large number of species transport equations. When the underlying assumptions are valid, the non-premixed approach is preferred over the finite rate formulation. This model can be used only when the reacting flow system meets several requirements. First, the flow must be turbulent. Second, the reacting system includes a fuel stream, an oxidant stream, and, optionally, a secondary stream (another fuel or oxidant, or a non-reacting stream). Finally, the chemical kinetics must be fast enough so that the flow is near chemical equilibrium. The mean combustion temperature of the simulated PDF is shown in Fig. 3.

If the value of the mean mixture fraction is zero and one, it represents air flow and fuel flow, respectively. As shown in Fig. 3, while the mean mixture fraction value is <0.1 , the average temperature could be as high as 2300 K.

The PRESTO and SIMPLE algorithms are employed in the present study for pressure interpolation and pressure–velocity coupling, respectively. The thermal properties of the species are given as functions of temperature and standard atmospheric pressure (1.013×10^5 Pa).

3.4 Model of heat transfer

All the required functions describing temperature changes, heat transfer, the kinetics of the volatile release, moisture evaporation and vapor condensation have been investigated with the ANSYS-Fluent software [14–16]. The model of the Uhde carbonization furnace is based on the following assumptions: (1) The

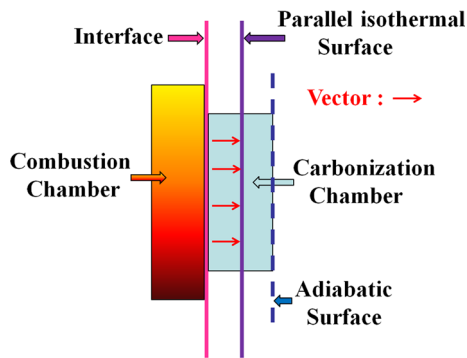


Fig. 4 The schematic of the “Vector”

process is two dimensional. (2) The lignite assumed to be porous. (3) The diffusion of the gas product is negligible. The mathematical model is established by considering the heat conduction process in solid materials. The solid’s coefficient of thermal conductivity, radiation heat-transfer, as well as the gas’s convection and radiation heat transfer coefficient were calculated, and fitted as a unified thermal conductivity coefficient. The solid within the model has no relative motion and the interior of it is without its own heat source. The energy equation and the enthalpy variable equation are shown in Eqs. (6) and (7) respectively. During the heat transfer process, the vector from the interface between the carbonization and combustion chamber to the parallel isothermal surface within the carbonization furnace was used to simulate the one-dimensional unsteady state heat conduction; The schematic of this “vector” was shown in Fig. 4. After considering the change of the thermal physical properties, we can formulate the approximate one-dimensional unsteady state heat conduction differential equations as shown in Eq. (8).

$$\frac{\partial(\rho h)}{\partial t} = \nabla \cdot (\kappa_{eff} \nabla T) \quad (6)$$

$$h = \int_{T_{ref}}^T C_p dT \quad (7)$$

$$\rho_{coal} C_{coal} \frac{\partial T}{\partial t} = \frac{\partial}{\partial x} \left(\lambda \frac{\partial T}{\partial x} \right) \quad (8)$$

Where κ_{eff} effective thermal conductivity (W/(m K)), h enthalpy (J/kg), ρ density (kg/m^3), C specific heat (J K/kg), T carbonization temperature ($^{\circ}\text{C}$), t carbonization time (sec or min), x heat transfer distance (mm or m).

The coefficient of effective thermal conductivity was imported into the heat transfer by the running program of the User-defined function (UDF) files.

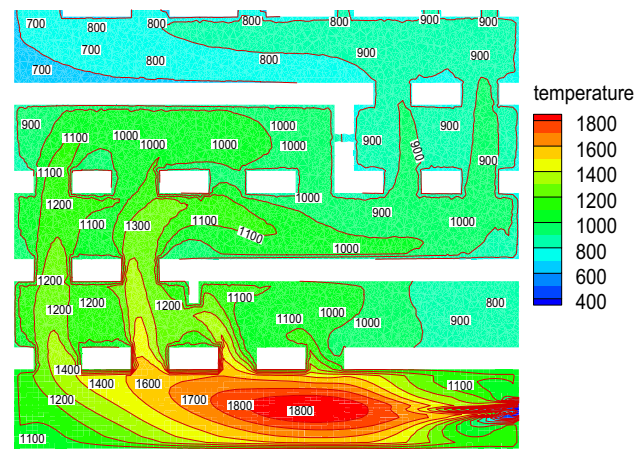


Fig. 5 Simulated temperature distribution in Uhde combustion chamber (Temperature:K)

4 Results and discussion

4.1 The optimization of the Uhde combustion chamber

4.1.1 The temperature distribution in the original Uhde combustion chamber

In the Uhde combustion chamber, COG of $32 \text{ m}^3/\text{h}$ and air of $175 \text{ m}^3/\text{h}$ were burned. The simulated temperature distribution is shown in Fig. 5. Before each experiment, a temperature calibrating instrument (FLUKE-714) was used to calibrate the thermocouples for the measurements.

As shown in Fig. 5, the high temperature concentrated in the first and second layer of the combustion chamber, and temperature distribution in the third, fourth and fifth layers was not uniform, failing to satisfy the industrial production of semi-coke. To test and verify the accuracy of our simulation results, with the same chamber set-up and working conditions, an experiment (actual combustion) was carried out. Combustion and boundary conditions were shown in Table 4. The thermocouple (type B) was used to measure temperature. Before every experiment, a temperature calibration took place.

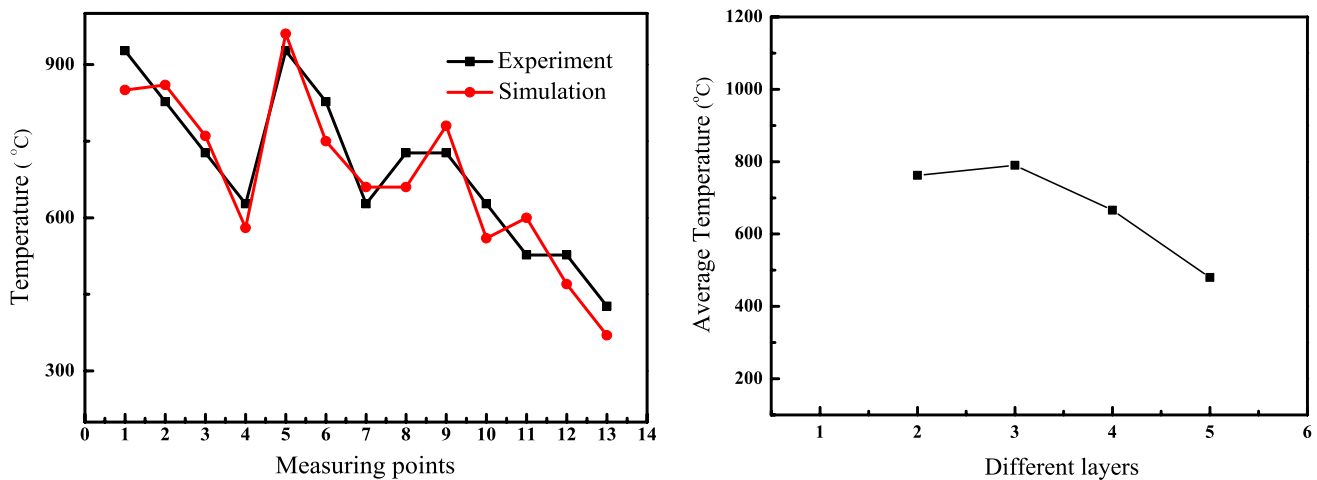
The bottom-left corner in Fig. 5 was set as the coordinate origin. As shown in Table 5, the points 1–4, 5–7, 8–10 and 11–13 were stand for the temperature measurement locations in the second, third, fourth and fifth layer of the original Uhde combustion chamber. The simulated temperature could be obtained via different horizontal and vertical positions in Fig. 5. The structure of the experimental combustion chamber was same to the simulated Uhde combustion chamber. And the combustion experiment was carried out at working condition 1. The experimental temperature of the corresponding points was obtained after the

Table 4 Combustion conditions and boundary conditions

Fuel	Working conditions	Structure of combustion chamber	Heat transfer conditions	Fuel pressure (KPa)	Excessive air coefficient	Gas flow (m ³ /h)	Air flow (m ³ /h)
COG	1	Uhde Circuted Flame path	Two-side Adiabatic	2.1	1.25	32	175

Table 5 The specific location of measuring points

Number	1	2	3	4	5	6	7	8	9	10	11	12	13
	Second layer				Third layer			Fourth layer		The fifth layer			
Location (mm)	x = 325	1000	1600	2200	300	1000	1900	650	1300	1950	650	1300	2300
	y = 610	610	610	610	1010	1010	1010	1410	1410	1410	1780	1780	1780

**Fig. 6** Temperature comparison chart in working condition 1

temperature stabilized for 10 h, and these data was compared with the simulation data, as shown in Fig. 6.

As shown in Fig. 6, the difference between experimental and simulated value is within 40–80 °C, indicating that the numerical calculation can successfully describe the real temperature distribution in the Uhde furnace. Both the vertical and horizontal temperature gradient in each layer vary considerably. The Uhde combustion chamber was then optimized to achieve a homogeneous temperature distribution and meet the industrial pyrolysis requirements. First, we changed the size and direction of the exhaust gas outlet in every flame path layer at the base of the chamber. Then we added our self built gas guide structure in the heat transfer section.

4.1.2 Structure optimization of the Uhde combustion chamber

To tackle problems existing in the combustion chamber (as shown in Fig. 5), the space of the chamber was reduced by

removing the fifth layer flame path. In addition, the structure of the heat transfer section was modified, the vertical space of heat transfer section was increased, and a special self-developed gas guide structure was installed. By adding our gas guide and increasing the height of the heat transfer section, the turbulence of the flue gas present in the heat transfer section could be increased, and create a more uniform high-temperature distribution. Furthermore, by reducing the height of the combustion chamber, we needed fewer silica bricks and the temperature could reach a uniform distribution easier in the smaller space. This is very helpful for industrial production. COG of 32 m³/h and air of 175 m³/h was burning in the combustion chamber. The simulated temperature distributions of different optimization plans are shown in Figs. 7, 8, 9, 10, 11.

By selecting the temperature of corresponding points in Figs. 7, 8, 9, 10, 11, we can get the vertical and horizontal temperature distribution of plan 1 to plan 5, as shown in Fig. 12. The bottom-left corner of each figure was set as the coordinate origin.

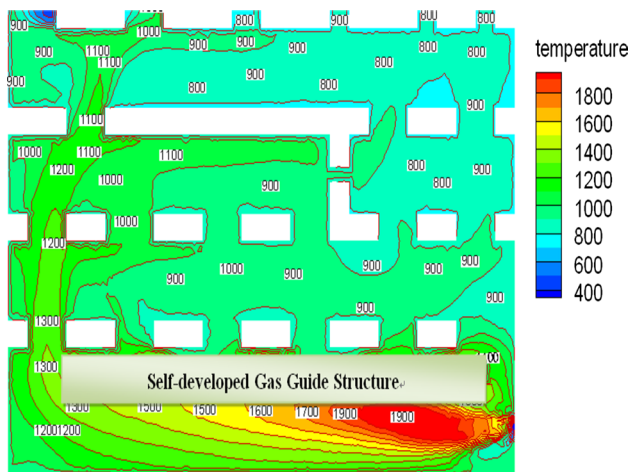


Fig. 7 The optimization plan 1

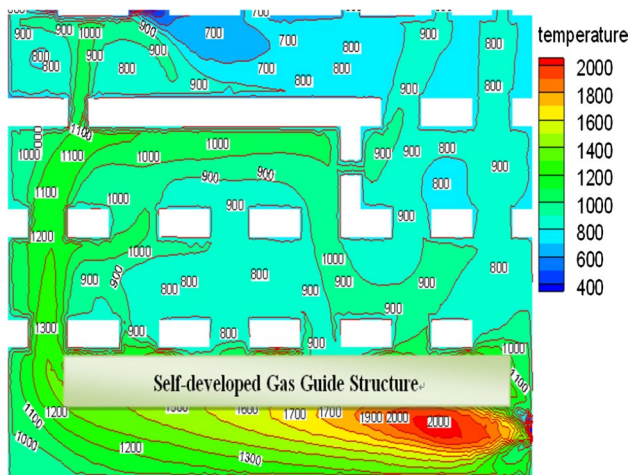


Fig. 8 The optimization plan 2

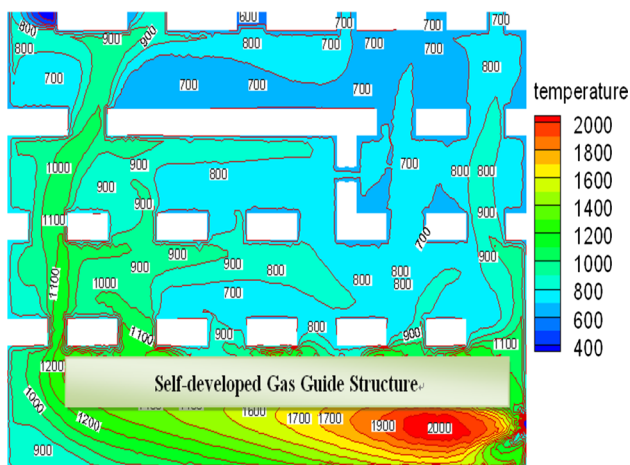


Fig. 9 The optimization plan 3

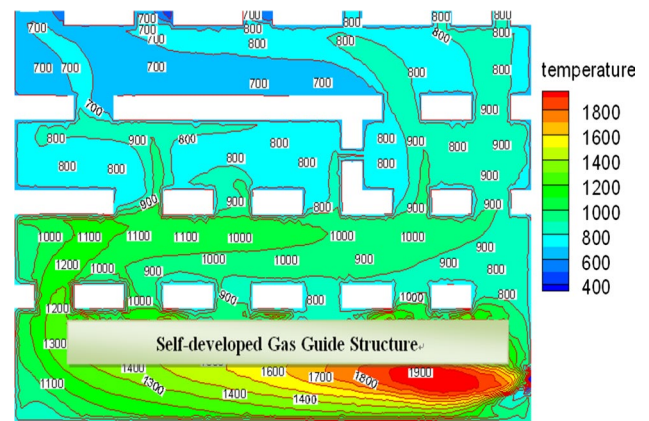


Fig. 10 The optimization plan 4

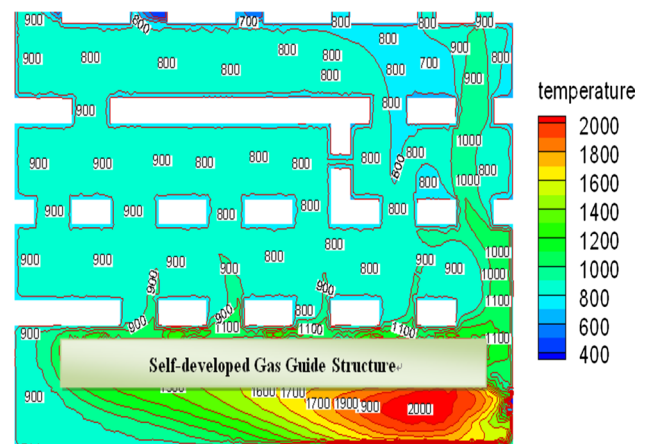


Fig. 11 The optimization plan 5

As shown in Fig. 12, comparing the horizontal and vertical temperature gradient, we can clearly see that: the horizontal temperature gradient arranged in the order of: Plan-1 > Plan-4 > Plan-3 > Plan-2 > Plan-5; the vertical temperature gradient arranged in the order of: Plan-4 > Plan-3 > Plan-2 > Plan-1 > Plan-5.

The horizontal and vertical temperature gradient of Plan-5 was the smallest and this combustion chamber could meet the industrial heat transfer requirements. So, Plan 5 was selected as the optimal structure.

4.1.3 Comparison between experiments and simulated results

For the optimized combustion chamber of plan 5, the burning experiments were carried out. The gas guide structure was installed in the heat transfer section and the optimized solution of plan 5 adopted in the pyrolysis section. At the same time, a carbonization furnace was built to investigate the heat

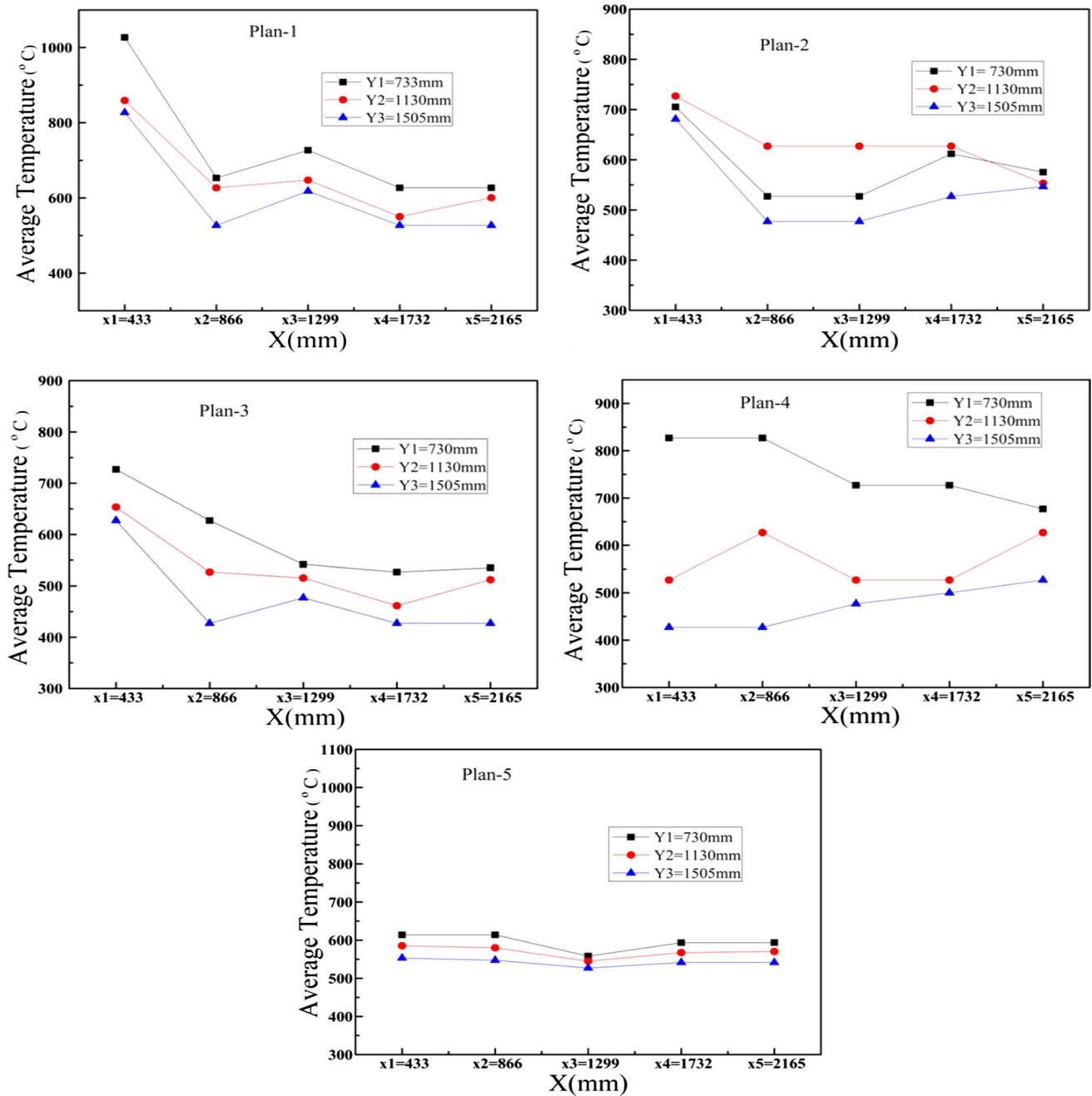


Fig. 12 Average temperature distribution of optimization Plan1–5

transfer. The experimental set-up of the carbonization furnace ($2600 \times 300 \times 1680$ mm) is shown in Fig. 13. Combustion conditions and boundary conditions are shown in Table 6. Temperature is measured by B-type thermocouples.

A chart comparing the simulated and experimental results is shown in Fig. 14. The points 1–5, 6–10 and 11–14 are the temperature measuring points in the second, third and fourth layer of the flame path respectively. The exact locations of these points in the two-dimensional rectangular coordinate system are shown in Table 7.

As can be seen from Fig. 14, the errors range for both experiment and simulation is 40–80 °C.

This suggests that the numerical simulation works well to describe the temperature distribution in optimized Uhd furnace. The horizontal and vertical temperature gradient was smaller than 100 °C. The average temperature of the different layers in the pyrolysis section equalizes and the overall temperature is about 600 °C. This means we meet the industrial criteria for low temperature pyrolysis with plan 5.

Fig. 13 Experimental set-up of the carbonization furnace

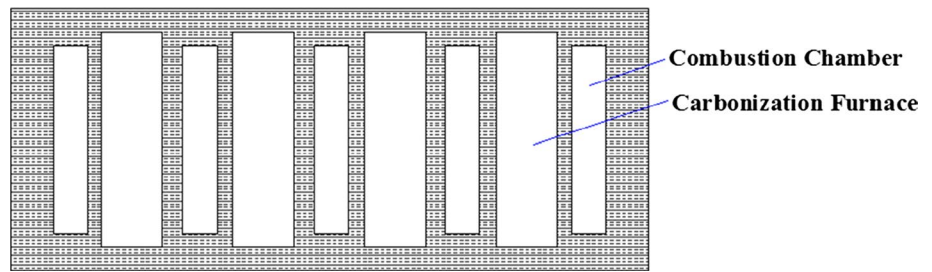


Table 6 Combustion and boundary conditions

Fuel	Working conditions	Structure	Heat transfer conditions	Pressure (KPa)	Air coefficient	Gas flow (m ³ /h)	Air flow (m ³ /h)
COG	2	Optimized Uhde furnace	One side adiabatic	2.1	1.25	32	175

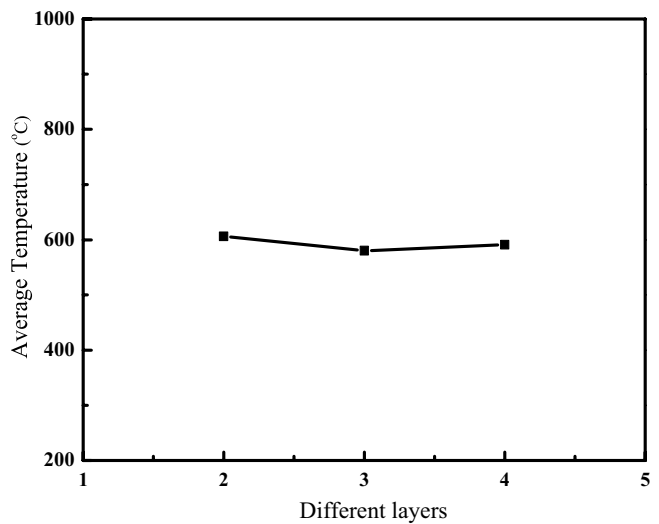
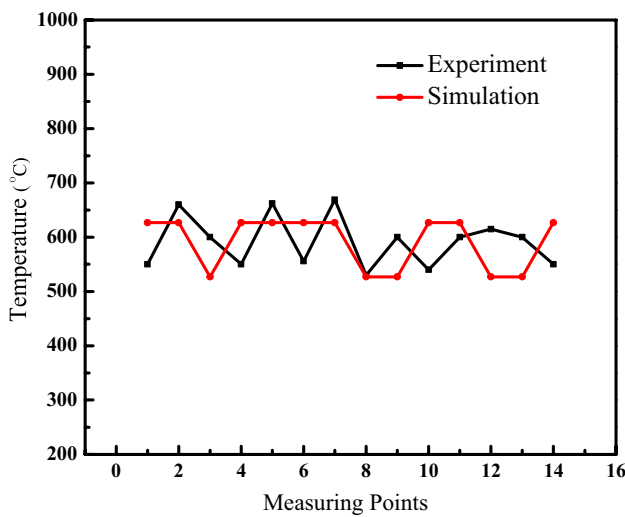


Fig. 14 Temperature comparison charts of working condition 2

Table 7 The specific location of measurement points

Number	1	2	3	4	5	6	7	8	9	10	11	12	13	14
	Second layer					Third layer					Fourth layer			
Location (mm)	x = 433	866	1299	1743	2165	433	866	1299	1732	2165	433	866	1500	2165
	y = 730	730	730	730	730	1130	1130	1130	1130	1130	1505	1505	1505	1505

4.2 Simulation results and experiment of heat transfer

The COG (flowing at 32 m³/h) was burned in the optimized combustion chamber together with air (flow rate 175 m³/h). After the temperature became stabilized, raw coal of Inner Mongolia lignite (grain size 10–15 mm) was delivered into the carbonization furnace. Unilateral heat

transfer was tested with the optimized circuit flame path combustion chamber. Variation trends of average temperature following the carbonization time are shown in Fig. 15 and the proximate and ultimate analysis of lignite and its semi-coke are shown in Table 8. The simulated temperature trends in the carbonization furnace at the measurement points are shown in Fig. 16. A comparison between

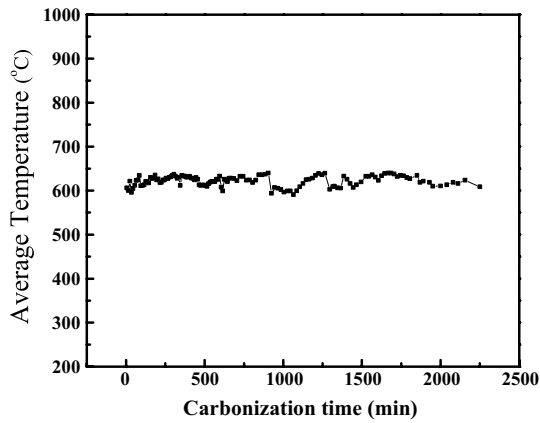


Fig. 15 Average temperature at the measurement points

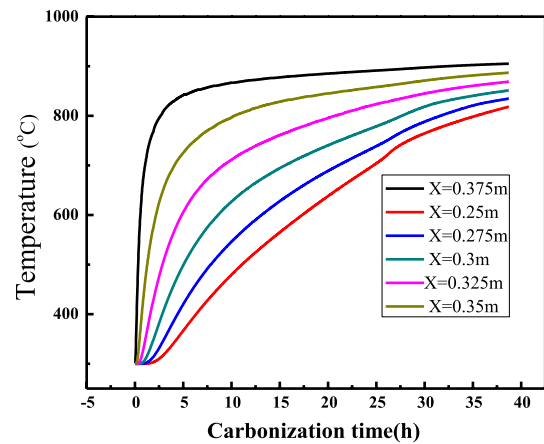


Fig. 16 Simulated temperature trends at the measurement points

the simulation and the experimental results ($x = 0.35 \text{ m}$) is shown in Fig. 17.

As can be seen from Fig. 16 and Fig. 17, during the process of combustion and heat transfer, the average temperature among corresponding points of the combustion chamber remains at 550–650 °C, which is a suitable heat source for low-temperature pyrolysis. The proximate and ultimate analysis (Table 8) of lignite semi-coke, taken from the middle of the carbonization furnace after 35 h, indicates that the low temperature pyrolysis of lignite had finished after this time. This by-product can meet the industrial requirements. At the same time, this confirms that the low-temperature combustion chamber and the produced semi-coke meet the industrial requirements for low-temperature pyrolysis. As shown in Fig. 17, the simulated temperature curve is consistent with the measured temperature curve.

Overall, this study can provide a theoretical framework to better understand and further optimize the lignite pyrolysis technology.

5 Conclusions

1. The results of the experiments described in this work aimed to solve the uneven temperature distribution existing in the industrial Uhde combustion chamber and to study the heat transfer properties within the low-temperature carbonization chamber. A CFD flow solver based on finite volume method (ANSYS-

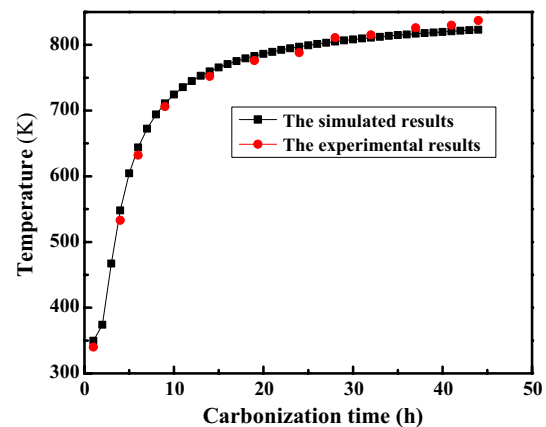


Fig. 17 Comparison between the simulated results and the experimental results ($x = 0.35 \text{ m}$)

2. The Realizable $k-\epsilon$ turbulence model, P-1 radiation model, and the Non-premixed combustion model are adopted to optimize the chamber, by adding our gas guide structure to the heat transfer section and adjusting the gas flow size in the flame path, the optimum structure was obtained. By adopting this optimum structure, the temperature distribution within the combustion chamber is now uniform and the average temperature can meet the conditions (500–650 °C) for low-temperature pyrolysis. Meanwhile, the simulation reflects the experimental results within an error range of 40–80 °C, which satisfying industrial requirements.

Table 8 Properties of the lignite and the semi-coke

Sample	Proximate analysis/wt%			Ultimate analysis/wt%, daf				
	Mad	Aad	Vdaf	C	H	O	N	S _t
NM lignite	18.60	11.83	50.44	72.10	3.85	22.27	1.52	0.26
Semi-coke	2.43	23.40	14.09	86.76	3.36	7.95	1.44	0.49

all suitable for simulating the temperature field distribution for the combustion of coke-oven gas and air in the combustion chamber.

3. The one dimensional unsteady state heat conduction differential equation $\rho_{coal} C_{coal} \frac{\partial T}{\partial t} = \frac{\partial}{\partial x} (\lambda \frac{\partial T}{\partial x})$ can be used to describe the heat transfer process. The calculated temperature curve in our study is consistent with the measured data. Our research of the optimized Uhde carbonization furnace provides a theoretical and technical basis for the lignite pyrolysis. Further studies are underway to properly model the heat transfer process in the low-temperature carbonization chamber, including water vapor migration and phase change effects, particle size of lignite as well as the thickness of carbonization furnace change effects, and to simulate more precisely the temperature distribution about lignite pyrolysis.

Acknowledgments This work was supported by the National Natural Science Foundation of China (Grant No. 51274147), National Science & Technology Pillar Program (Grant No.2012BAA04B03), Shanxi Provincial Natural Science Foundation (2010011014-1) and Shanxi Returned Students Fund (1999-018).

References

1. Wang N, Zhu S (2010) A study on the pyrolysis characters of Baoril lignite and its product property. *China Coal* 36:85–89
2. Ma ZY, Liu ZQ, Miao WH (2011) Research on the design and application of new technology of low temperature drying distillation with lignite. *Coal Qual Technol* 3:54–56
3. Wang WQ (2012) A brief meaning of quality improvement of lignite. *Shanxi Chem Ind* 32:44–46
4. Chu M, Gao JJ (2012) Experiment study on low temperature pyrolysis upgrading of lignite. *Coal Sci Technol* 40:95–99
5. Chi YL, Li SY, Yue CT, Ding KL (2005) Properties of Zhaotong lignite and its pyrolysis products. *J Univ Pet* 29:101–106
6. Zhang HR, Zhang YF (2011) An overview of LFC and ACCP process. *Energy Energy Conserv* 65:71–74
7. Sass A (1974) Garrett's coal pyrolysis process. *Chem Eng Prog* 70:72–73
8. Chen L, Zhang YF, Liu J, Wang Y, Xu Y, Wang Y (2013) R&D on low-temperature carbonization technology of low-rank coal with efficient tar recovery (I) The present situation and development of efficient tar recovery technology. *Chem Ind Eng Prog* 32:2343–2534
9. Liu J, Zhang YF, Wang Y, Chen L, Xu Y, Zhao HB (2013) R&D on low-temperature carbonization technology of low-rank coal with efficient tar recovery(II) Temperature distribution simulation and structural optimization of the low-temperature combustion chamber in carbonization furnace. *Chem Ind Eng Prog* 32:2112–2119
10. Bao LG, He BW (1992) A continuous and vertical carbonization oven with circuited flame path: China [P]. 91210011.7
11. Łukasz S, Adam F, Zbigniew BS, Andrzej JN, Ludwik K, Grzegorz Ł (2015) CFD model of the coal carbonization process. *Fuel* 150:415–424
12. Wei L, Feng YH, Zhang XX (2015) Numerical study of volatiles production, fluid flow and heat transfer in coke ovens. *Appl Therm Eng* 81:353–358
13. Raiee SE, Ayenehpour S, Sadeghiazad MM (2015) A study on the optimization of the angle of curvature for a Ranque-Hilsch vortex tube, using both experimental and full Reynolds stress turbulence numerical modeling. *Heat Mass Transf*. doi:10.1007/s00231-015-1562-y
14. Wang JM, Peng F (2004) Numerical simulating and optimization for three-dimensional flow and combustion of burner. *J Wuhan Univ Technol* 26:79–82
15. Lu XF, Li YQ (2011) Study on structure improvement of the burner based on CFD. *Acta Petrollet Sinica (Pet Process Sect)* 27:787–791
16. Hu GH, Wang HG, Qian F (2011) Numerical simulation on flow, combustion and heat transfer of ethylene cracking furnaces. *Chem Eng Sci* 66:1600–1611
17. Nathan MK, Prasanna S, Muthuveerappan G (2000) Three-dimensional mesh generation using principles of finite element method. *Adv Eng Softw* 31:25–34
18. Fluent Inc. (2003) *Fluent users guide* [M]. USA
19. Coking Design Reference Editorial Group (1978) *Coking design reference* [M]. Press of Metallurgy Industry, Beijing, pp 125–126
20. Wang FJ (2004) *Computational fluid dynamics analysis* [M]. Tsinghua University Press, Beijing, pp 217–223
21. Liu NS, Shih THS (2006) Turbulence modeling for very large-eddy simulation. *Aiaa J* 44:687–697
22. Nathan MK, Prasanna S, Muthuveerappan G (2000) Three-dimensional mesh generation using principles of finite element method. *Adv Eng Softw* 31:25–34
23. Sazhin SS, Sazhina EM, Faltsi-Saravelou O, Wild P, Sazhina EM (1996) The P-1 model for thermal radiation transfer: advantages and limitations. *Fuel* 75:289–294
24. Siegel R, Howell JR (1992) *Thermal radiation heat transfer* [M]. Hemisphere Publishing Corporation, Washington (DC), pp 175–186
25. Elattar HF, Stanev RK, Specht E, Fouda A (2014) CFD simulation of confined non-premixed jet flames in rotary kilns for gaseous fuels. *Comput Fluids* 102:62–73
26. Carbonell D, Perez-Segarra CD (2009) Flamelet mathematical models for non-premixed laminar combustion. *Combust Flame* 156:334–347
27. Lotfi Z, Abila C (2013) Numerical simulations of non-premixed turbulent combustion of CH₄-H₂ mixtures using the PDF approach. *Int J Hydrog Energy* 38:85–97